Synthesis, characterization and reactivity of tetranuclear ruthenium hydrido clusters containing chiral phosphine ligands

Viktor Moberg,[a] Pertti Homanen,[a] Simona Selva,[b] Roger Persson,[a] Matti Haukka,[c] Tapani A. Pakkanen,[c] Magda Monari*[b] and Ebbe Nordlander*[a]

Received 27th October 2005, Accepted 28th October 2005
First published as an Advance Article on the web 21st November 2005
DOI: 10.1039/b515273a

The chiral clusters $[H_4Ru_4(CO)_{12-n}(L)_n]$ ($n = 1, 2$; L = NMDPP), 1,1-$[H_4Ru_4(CO)_{10}(L–L)]$ (L–L = DUPHOS, DIPAMP), 1,2-$[H_4Ru_4(CO)_{10}(DIOP)]$ and $[\{H_4Ru_4(CO)_{10}(DIOP)\}_2]$ have been synthesized by derivatizing the parent carbonyl cluster $[H_4Ru_4(CO)_{12}]$ with the appropriate mono- or didentate chiral phosphine ligand. The phosphine-substituted clusters were found to be able to catalyze the (asymmetric) hydrogenation of tiglic acid albeit with relatively low selectivity (enantiomeric excesses varying from 0 to 23%). It was found that the stability of the chiral ruthenium hydride clusters and the product distribution obtained in the catalytic reactions are dependent on the nature of the chiral phosphine. The crystal structures of $[H_4Ru_4(CO)_{12-n}(L)_n]$ ($n = 1, 2$; L = NMDPP), 1,1-$[H_4Ru_4(CO)_{10}(L–L)]$ (L–L = DUPHOS, O-DUPHOS (partially oxygenated ligand), DIPAMP), 1,2-$[H_4Ru_4(CO)_{10}(DIOP)]$ and $[\{H_4Ru_4(CO)_{10}(DIOP)\}_2]$ are presented.

Introduction

Asymmetric hydrogenation reactions are predominantly catalysed by Rh- and Ru-based catalysts. In the case of Rh(I)-containing catalysts,[1] enantioselectivities have been found to be dependent on the substrate used,[1] and the most frequently reported results for asymmetric hydrogenations affording high enantiomeric excesses (ee) involve unsaturated carboxylic acids with α-acylamido groups.[1,2] Systematic studies of Ru(II) complexes derivatized with chiral diphosphines have led to the discovery of highly active catalysts of the type $[Ru(O_2CR)_2(L_2)]$,[3] (L_2 = BINAP derivative; R = CH_3 or $C(CH_3)_3$), which are much less sensitive to the double bond geometry and the substituents present in the substrate. Despite the excellent results obtained with mononuclear ruthenium complexes, relatively few studies have been carried out on asymmetric catalysis based on phosphine-derivatized ruthenium clusters. Notable exceptions are the tetranuclear ruthenium hydrido clusters of the general formulas $[H_4Ru_4(CO)_{10}(L–L)]$ or $[H_4Ru_4(CO)_8(L–L)_2]$ (L–L = chiral bidentate phosphine).[4] These clusters have been used as catalysts for several asymmetric reactions, including isomerization,[5] hydroformylation,[6] and homogeneous hydrogenation[5] of various carboxylic acids. In the application of such clusters to asymmetric hydrogenation of tiglic acid (*trans*-2,3-dimethylacrylic acid; *trans*-2-methyl-2-butenoic acid) the enantiomeric discrimination and the catalyst activity have been reported to depend on the chiral phosphines coordinated to parent clusters, and hydrogenation under relatively harsh reaction conditions result in the formation of *S*- and *R*-forms of 2-methylbutyric acid with enantiomeric excesses (ee) that vary from 6–39%.[7] In an earlier study, we have shown that higher ee's and high conversion rates can be obtained under relatively mild reaction conditions when $[H_4Ru_4(CO)_{10}(x\text{-BDPP})]$ (x = *R*,*R*- or *S*,*S*-) is used as a catalyst.[8] Furthermore, the predominating enantiomeric form of the hydrogenated acid was shown to strongly depend on the chiral conformation of the cluster-coordinated bis-2,4-(diphenylphosphino)pentane (BDPP) ligand. In order to study the effect of cluster-coordinated chiral phosphines on the stability of modified tetranuclear ruthenium species, as well as the product distribution(s) in asymmetric hydrogenation reactions, we are currently studying the reactivity of a number of ruthenium clusters containing chiral ligands. Here, we describe the synthesis and characterization of new tetranuclear ruthenium hydrido clusters containing the chiral mono- and/or didentate phosphine ligands (*S*)-(+)-neomenthyldiphenylphosphine (NMDPP), 1.2-bis[(2*R*,5*R*)-2,5-dimethylphospholano]benzene (DUPHOS), (4*R*,5*R*)-(−)-*O*-isopropylidene-2,3-dihydroxy-1,4-bis(diphenylphosphino)-butane (DIOP), and (1*R*,2*R*)-bis{(2-methoxyphenyl)phenylphosphino}ethane (DIPAMP, Fig. 1), and we report the performance of the clusters in catalytic asymmetric hydrogenation of tiglic acid.

Experimental

General experimental procedures

All reactions were carried out under nitrogen atmosphere and manipulations of the products were performed in air. All solvents used in syntheses and catalysis tests were distilled under nitrogen and dried prior to use. Infrared spectra were measured using a Nicolet Avatar 360 FT-IR spectrometer with the appropriate solvent as background. ^{1}H and ^{31}P NMR spectra were recorded at 298 K on a Varian Unity 300 MHz spectrometer with $CDCl_3$ used as solvent and ^{31}P NMR shifts were referenced to external H_3PO_4 (85%). Thin-layer chromatography (TLC) was performed

[a]*Inorganic Chemistry, Center for Chemistry and Chemical Engineering, Lund University, Box 124, SE-221 00, Lund, Sweden. E-mail: Ebbe.Nordlander@inorg.lu.se; Fax: +46 46 222 4439*
[b]*Dipartimento di Chimica "G. Ciamician", Università di Bologna, via Selmi 2, I-40126, Bologna, Italy*
[c]*Department of Chemistry, University of Joensuu, BOX 111, FIN-80101, Joensuu, Finland*

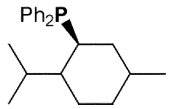

((1*S*)-2-isopropyl-1,5-dimethylcyclohexyl)-diphenylphosphine (NMDPP)

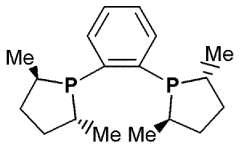

(2*R*,5*R*)-2,5-dimethyl-1-(2-((2*R*,5*R*)-2,5-dimethylphospholan-1-yl)-phenyl)phospholane (DuPHOS)

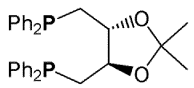

(4*R*,5*R*)-2,2-dimethyl-4,5-bis((diphenylphosphino)-methyl)-1,3-dioxolane (DIOP)

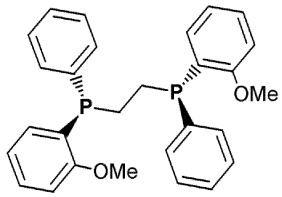

1,2-bis((2-methoxyphenyl)(phenyl)-phosphino)ethane (DIPAMP)

Fig. 1 Structures of the chiral phosphine ligands used in this investigation.

on commercial 20 × 20 cm plates covered with Merck Kiselgel 60 F254 to 0.25 mm thickness. HPLC purifications were carried out on a Rainin Dynamax chromatograph equipped with a reverse phase Dynamax C18 100 Å column, with acetonitrile used as the mobile phase. In the catalysis experiments, a Parr autoclave with PTFE lining ($V = 20$ mL) was used as the reaction vessel. The reagents were of analytical grade and were used as received. The chiral phosphines were enantiomerically pure samples that were purchased from STREM Chemicals (DUPHOS and DIOP) and from Larodan Fine Chemicals AB (NMDPP and DIPAMP). Tiglic acid, 2-methylbutyric acid (in pure *S*-form as well as a racemic mixture), and (*S*)-methyl mandelate were purchased from Sigma-Aldrich. The parent ruthenium cluster $[H_4Ru_4(CO)_{12}]$ was synthesized following the method of Kaesz and co-workers[9] and its purity was assessed using TLC and IR spectroscopy.

Preparation of $[H_4Ru_4(CO)_{11}(NMDPP)]$ (1) and $[H_4Ru_4(CO)_{10}(NMDPP)_2]$ (2)

Method A: Thermal ligand substitution. A mixture of $[H_4Ru_4(CO)_{12}]$ (85 mg, 0.11 mmol), NMDPP [= (*S*)-(+)-neomenthyldiphenylphosphine] (75 mg, 0.23 mmol) and toluene (30 mL) was placed in a 250 mL flask, and heated for 24 h at 85 °C under N_2. The resulting orange–red solution was dried under vacuum, dissolved in a small amount of a dichloromethane–hexane solution and separated using TLC. Elution with a dichloromethane–hexane mixture (1 : 1 v/v) gave a yellow–orange and an orange band as well as minor yellow and red fractions that were obtained in very low yield and were not characterized. The two main products were collected and extracted from silica with dichloromethane, dried under N_2 and identified as $[H_4Ru_4(CO)_{11}(NMDPP)]$ **1** (46 mg, 41%) as a yellow–orange solid (Anal. Found: C, 37.6; H, 3.3. Calc. for **1**: C, 38.1; H, 3.2%); $\nu_{CO}(CH_2Cl_2)/cm^{-1}$: 2092m, 2081m, 2063s, 2055vs, 2026s, 2006s, 1952w; ^1H NMR (hydride resonances): −17.4 (d); $^{31}P\{^1H\}$ NMR: 42.6 (s); *m*/*z* (FAB): 1044 ($M^+ + 3$) and $[H_4Ru_4(CO)_{10}(NMDPP)_2]$ **2** (60 mg, 37%) isolated as an orange solid (Anal. Found: C, 46.6; H, 4.6. Calc. for **2**: C, 46.45; H, 4.5%); $\nu_{CO}(CH_2Cl_2)/cm^{-1}$: 2079w, 2064w, 2048s, 2023vs, 1994s, 1959m; ^1H NMR (hydride resonances): −17.0 (d); $^{31}P\{^1H\}$ NMR: 40.1 (s); *m*/*z* (FAB): 1339 ($M^+ + 2$). Crystallization of the products from dichloromethane–hexane solutions yielded yellow–orange and orange crystals suitable for X-ray diffraction analysis.

Method B: Oxidative decarbonylation. The same products could also be obtained using a dichloromethane–acetonitrile mixture (2 : 1) as a solvent in the presence of Me_3NO. The same stoichiometric ratios and scale of reactants were reacted with a slight excess of Me_3NO at room temperature. The isolation/purification and yields of the products were identical to those described above. Yields: **1** (31 mg, 27%) and **2** (20 mg, 14%).

Preparation of 1,1-$[H_4Ru_4(CO)_{10}(DUPHOS)]$ (3) and 1,1-$[H_4Ru_4(CO)_{10}(O\text{-}DUPHOS)]$ (4)

Method A: Thermal substitution. $[H_4Ru_4(CO)_{12}]$ (60 mg, 80 μmol) and DUPHOS [(−)-1,2-bis((2*R*,5*R*)-2,5-dimethylphospholano)benzene] (37 mg, 0.12 mmol) were added to 30 mL of toluene and the solution was heated at 85 °C for 24 h under nitrogen. The resulting orange–red mixture was dried under vacuum, extracted with a small amount of dichloromethane and separated with TLC (eluent: dichloromethane–hexane 1 : 1 v/v). The main band was a stationary brownish-black front, most likely a decomposition product of the parent cluster. Two minor bands were separated from the TLC plates, extracted from silica with dichloromethane and dried under vacuum. The first yellow fraction was identified as the unreacted parent cluster and the second orange fraction was identified as 1,1-$[H_4Ru_4(CO)_{10}(DUPHOS)]$ **3** (8 mg, 10%) (Anal. Found: C: 33.7; H: 3.34. Calc. for **3**: C: 33.7; H: 3.23%); $\nu_{CO}(CH_2Cl_2)/cm^{-1}$: 2073s, 2041vs, 2018vs, 1998s, 1981m br, 1950sh br; ^1H NMR (hydride resonances): −15.3 (br), −16.2 (br), −19.6 (t); $^{31}P\{^1H\}$ NMR: −3.4 (d), −12.8 (d); *m*/*z* (FAB): 996 ($M^+ + 2$). Single crystals suitable for X-ray diffraction analysis were obtained by recrystallization from a dichloromethane–hexane solution.

Cluster **3** was also formed when the ligand substitution reaction was tested in refluxing THF. After TLC separation, the red–orange product (spectral data similar to those of **3**) was recrystallized from dichloromethane. In addition to an orange microcrystalline powder of **3**, a few red crystals were formed, which were analyzed by single-crystal X-ray diffraction (*vide infra*) and identified as $[H_4Ru_4(CO)_{10}$(O-DUPHOS)] **4**, containing partially oxygenated chelating diphosphine ligand. Because of the very poor yield, no spectroscopic data for this compound are available (attempts to resynthesize compound **4** have failed).

Method B: Oxidative decarbonylation. Cluster **3** could also be obtained by reaction of $[H_4Ru_4(CO)_{12}]$ with Me_3NO in the presence of DUPHOS. The reaction was carried out at room temperature in a dichloromethane–acetonitrile mixture (2 : 1) using the same stoichiometric ratios and scale of reactants as above, with dropwise addition of a slight excess of Me_3NO. The isolation/purification of **3** was identical to that described above (yield: 63 mg, 80%).

Preparation of 1,2-$[H_4Ru_4(CO)_{10}$(DIOP)] (5) and $[\{H_4Ru_4(CO)_{10}(\mu$-DIOP)$\}_2]$ (6)

A total of 40 mg (54 μmol) of $[H_4Ru_4(CO)_{12}]$ and 32.2 mg (65 μmol) of DIOP [= (4*R*,5*R*)-(−)-*O*-isopropylidene-2,3-dihydroxy-1,4-bis(diphenylphosphino)butane] were dissolved in 10 ml of CH_2Cl_2 and 7 ml of CH_3CN and the solution was stirred at room temperature. A slight excess of Me_3NO (9.75 mg, 0.13 mmol) dissolved in 3 ml of CH_3CN was added dropwise and very slowly to the stirred solution. The initial deep yellow solution darkened and changed colour to deep red during the addition of Me_3NO. After 2 h the solvent was evaporated under vacuum. The resultant residue was subjected to preparative TLC, using *n*-hexane–CH_2Cl_2 (1 : 1 v/v) as eluent, to give two main bands which were extracted with CH_2Cl_2. A dark orange band ($R_f = 0.75$), identified as 1,2-$[H_4Ru_4(CO)_{10}$(DIOP)] **5** (33 mg, 51%) $\nu_{CO}(CH_2Cl_2)/cm^{-1}$: 2071s, 2051s, 2029vs, 2009s, 1964w, 1945w; ^1H NMR (hydride resonances): −16.8 (s, br), −16.9 (d), −17.4 (s), −17.7 (m); $^{31}P\{^1H\}$ NMR: 16.9 (s), 23.4 (s) 24.7 (s), 26.7 (s) (J_{P-P} not resolved), and a dark yellow band ($R_f = 0.8$), identified as $[\{H_4Ru_4(CO)_{10}(\mu$-DIOP)$\}_2]$ **6** (10 mg, 8%) $\nu_{CO}(CH_2Cl_2)/cm^{-1}$: 2074s, 2055vs, 2016s, br, 1992m, br, 1951w, 1934w; ^1H NMR (hydride resonances): −17 ppm (m); $^{31}P\{^1H\}$ NMR: 29.6 (s). Red crystals of **5** were obtained by slow evaporation of a $CHCl_3$ solution and the yellow product **6** was crystallized from *n*-hexane–CH_2Cl_2 (2 : 1).

Preparation of 1,1-$[H_4Ru_4(CO)_{10}$(DIPAMP)] (7) and 1,2-$[H_4Ru_4(CO)_{10}$(DIPAMP)] (8)

Method A: Oxidative decarbonylation. A total of 55 mg (74 μmol) of $[H_4Ru_4(CO)_{12}]$ and 36 mg (78 μmol) of DIPAMP [= (1*R*,2*R*)-bis{(2-methoxyphenyl)phenylphosphino}ethane] were dissolved in a mixture of dichloromethane–acetonitrile (10/10 mL). A small excess of Me_3NO (9 mg, 0.12 mmol) dissolved in 5 ml acetonitrile was added dropwise over a period of 30 min to the stirred cluster/ligand solution. The initial yellow coloured solution turned into deep red during the addition of Me_3NO. The reaction was monitored continuously by spot TLC (dichloromethane–hexane 2:3 v/v) and when no parent cluster could be observed (3 h), the solvent was removed under vacuum. The resulting red solid was dissolved in a small quantity of dichloromethane (2 mL) and separated using preparative TLC (eluent dichloromethane–hexane 2 : 3 v/v). In addition to a stationary brown band (decomposition product(s)) three bands were separated from the TLC plates, extracted from silica with dichloromethane and dried under vacuum. The first yellow fraction was identified as the unreacted parent cluster and the second, orange, and the third, red, fractions were identified as phosphine-substituted 1,1-$[H_4Ru_4(CO)_{10}$(DIPAMP)] **7** (3 mg, 3%) ^1H NMR (hydride resonances): −14.9 (br), −16.1 (br), −19.2 (s); ^{31}P NMR: 72.4; $\nu_{CO}(CH_2Cl_2)/cm^{-1}$ 2072s, 2042vs, 2017vs, 1999s, 1980m, 1948w; *m/z* (FAB): 1148 (M^+), and 1,2-$[H_4Ru_4(CO)_{10}$(DIPAMP)] **8** (36 mg, 43%) ^1H NMR (hydride resonances): −17.3 (br s); ^{31}P NMR: 32.8; ν_{CO} $(CH_2Cl_2)/cm^{-1}$ 2069m, 2048s, 2025vs, 2003m, 1980w, 1959w; *m/z* (FAB) 1149 ($M^+ + 1$). Orange crystals of **7** were obtained by slow evaporation of dichloromethane–hexane at 4 °C.

Method B: Thermal ligand substitution at high pressure. Clusters **7** and **8** could also be synthesized in good yields using an autoclave. A total of 90 mg (0.12 mmol) of $[H_4Ru_4(CO)_{12}]$ and 68 mg (0.15 mmol) of DIPAMP was suspended in 10 mL of an ethanol–toluene mixture (1 : 1 v/v) and transferred to the autoclave. The vessel was closed firmly and pressurized with 50 bar of hydrogen gas, after being purged four times at 20 bar. The reaction mixture was stirred with a magnetic stirrer and heated at 104 °C (actual inside temperature) for 22 h. The autoclave was allowed to cool down to room temperature and then opened carefully. The color of the solution had changed from yellow to dark red/orange. The reaction mixture was reduced under vacuum to approx. 2–3 mL and separated using preparative TLC (eluent dichloromethane–hexane 2 : 3 v/v). In addition to a stationary brown band (decomposition product(s)), three bands were separated from the TLC plates, extracted from silica with dichloromethane and dried under vacuum. The first yellow fraction was identified as the unreacted parent cluster and the second, orange, and the third, red, fractions were identified as phosphine-substituted 1,1-$[H_4Ru_4(CO)_{10}$(DIPAMP)] **7** (56 mg, 41%) and 1,2-$[H_4Ru_4(CO)_{10}$(DIPAMP)] **8** (11 mg, 8%), respectively.

Catalysis experiments

In a typical reaction, an autoclave was loaded with catalyst and substrate under N_2, and the degassed solvent mixture was added (2.5 mL EtOH/2.5 mL toluene). The reaction vessel was closed and purged several times with hydrogen before final pressurizing to 50 bar. The reaction mixture was continuously stirred with a magnetic stirrer (*ca.* 850 rpm) and heated at 100 °C for 24, 48 or 72 h. After a cooling period of approx. 30 min., the reaction vessel was carefully depressurized and opened. The homogeneous reaction mixture was transferred to a 50 mL flask and concentrated under vacuum. The conversions for the catalysis runs were calculated on the basis of NMR analyses. Samples for NMR were taken both before and after concentration of the reaction mixture. The cluster species and 2-methyl butyric acid were separated from the concentrated sample using HPLC, and analyzed by IR and NMR spectroscopies. The enantiomeric excess of the product was determined by derivatizing 2-methylbutyric acid with (*S*)-methyl mandelate and analyzing the diastereomeric product mixture by NMR, as described by Tyrrell *et al.*[10]

X-Ray data collection and structure solutions

The diffraction data for **1–4** were collected using a Nonius Kappa CCD diffractometer. The Denzo and Scalepack programs[11] were used for cell refinements and data reductions. The diffraction data for **5–7** were collected using a Bruker-AXS SMART CCD diffractometer. The initial cell parameters and an orientation matrix were obtained from least-squares refinement on reflections measured in three different sets of 20 frames each, in the range $-15 < \theta < 15°$. The intensity data comprising a full sphere were collected using the ω-scan technique with frame width set at 0.3°. The structures of **1–7** were solved using the SIR97[12] or SHELXS 97 programs,[13] and refined with full-matrix least-squares on F_o^2 using SHELXTL.[14] Anisotropic displacement parameters were assigned to all non-hydrogen atoms in the structure. All hydrogens except the hydrides were placed in idealized positions. The positions of the hydrides for **1–4** were calculated using the XHYDEX program.[15] The hydrides for **5** and **6** were experimentally located and their locations were confirmed by the XHYDEX program. The absolute structures for complexes **1–7** were determined on the basis of the absolute structure parameter (Flack index)[16] during the refinement process. Clusters **2**, **5**, **6** and **7** crystallize as solvated $[H_4Ru_4(CO)_{10}(NMDPP)_2]\cdot CH_2Cl_2$, $[H_4Ru_4(CO)_{10}(DIOP)]\cdot 0.6CHCl_3$, $[\{H_4Ru_4(CO)_{10}(DIOP)\}_2]\cdot 1.6C_6H_{14}$ and 1,1-$[H_4Ru_4(CO)_{10}(DIPAMP)]\cdot 0.4H_2O$. Cluster **3** crystallizes in the space group $P2_12_12_1$, with two independent molecules (A and B) in the asymmetric unit. The crystallographic data for the reported clusters are collected in Table 1.

CCDC reference numbers 287842–287848.

For crystallographic data in CIF or other electronic format see DOI: 10.1039/b515273a

Results and discussion

Cluster synthesis

In order to obtain good yields of the phosphine-substituted tetraruthenium clusters, the coordination of the phosphine ligands *via* both thermal and oxidative decarbonylation of the parent cluster was investigated. The optimal synthetic method was found to vary with the nature of the phosphine and the reaction conditions. In general, thermal ligand substitution reactions were inefficient when solvents with relatively low boiling points were used. For the monodentate phosphine NMDPP, thermal substitution in refluxing toluene gave the best yields and led to the formation of an approximate 1 : 1 mixture of the mono- and disubstituted products $[H_4Ru_4(CO)_{11}(NMDPP)]$ (**1**) and $[H_4Ru_4(CO)_{10}(NMDPP)_2]$ (**2**) (Fig. 2; combined yield *ca.* 70%). When the same reaction was carried out in a dichloromethane/acetonitrile solution using Me_3NO as a decarbonylation reagent, the yields were markedly lower and the product distribution changed to yield a 2 : 1 mixture of mono- and disubstituted species (combined yield *ca.* 40%).

In contrast, the diphosphine DUPHOS could be most efficiently coordinated to $[H_4Ru_4(CO)_{12}]$ by oxidative decarbonylation of the parent cluster. Only the disubstituted cluster 1,1-$[H_4Ru_4(CO)_{10}(DUPHOS)]$ (**3**) was isolated, although usually several minor products/fractions were observed upon purification of the product with TLC. Higher ligand to cluster molar ratios gave the same result. Thermal ligand substitution reactions in refluxing toluene led to extensive decomposition of the starting materials, also when reactions were carried out under H_2 atmosphere. Further attempts to coordinate DUPHOS to the parent cluster in refluxing THF caused partial oxidation of the diphosphine ligand, most likely because of the presence of peroxides or residual water in the solvent. The cluster 1,1-$[H_4Ru_4(CO)_{10}(O\text{-}DUPHOS)]$ (**4**), which contains a six-membered chelate ring, could be separated by fractional crystallization from the reaction mixture, mainly containing cluster **3**, and was characterized by single-crystal X-ray diffraction analysis (*vide infra*).

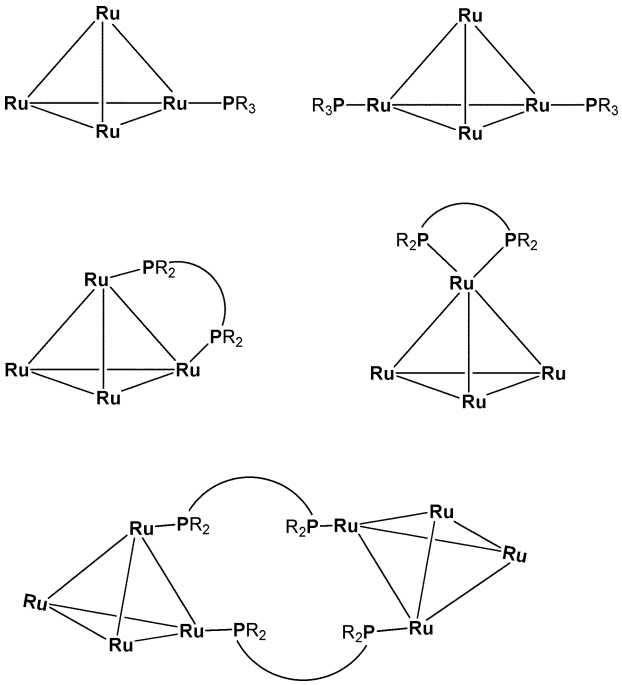

Fig. 2 Schematic structures of the phosphine coordination modes in the new ruthenium clusters that have been prepared in this study.

Whereas only the 1,1-isomer of $[H_4Ru_4(CO)_{10}(DUPHOS)]$ could be isolated, the analogous reaction with DIOP led to the formation of the corresponding 1,2-isomer, 1,2-$[H_4Ru_4(CO)_{10}(DUPHOS)]$ (**5**), in which the DIOP ligand bridges one Ru–Ru edge. It appears that the formation of the eight-membered "dimetallacycle" that results from the coordination of DIOP in **5** is favoured over the corresponding seven-membered metallacycle that would be formed if the phosphine were to coordinate in the chelate mode found in the 1,1-isomer. In addition to **5**, the dimeric cluster $[\{H_4Ru_4(CO)_{10}(\mu\text{-}DIOP)\}_2]$ (**6**) could be isolated as a minor product in the above-mentioned reaction. In the latter cluster, the coordination of the phosphorus donor atoms to the H_4Ru_4 framework differs from what is found in **5** and other similar tetraruthenium diphosphine clusters in the respect that the two phosphorus atoms are in axial and equatorial positions relative to each other (*vide infra*). The isolation of **6** provides further indirect evidence for the DIOP ligand preferring to coordinate in a bridging rather than chelating mode.

Reasonably good yields were obtained *via* both thermal substitution and oxidative decarbonylation when the diphosphine DIPAMP was coordinated to $[H_4Ru_4(CO)_{12}]$. The most striking feature was the difference in the product distribution. Thermal decarbonylation gave mainly the cluster 1,1-$[H_4Ru_4(CO)_{10}(DIPAMP)]$

Table 1 Crystallographic data for $[H_4Ru_4(CO)_{11}(NMDPP)]$ (**1**), $[H_4Ru_4(CO)_{10}(NMDPP)_2]\cdot CH_2Cl_2$ (**2**), 1,1-$[H_4Ru_4(CO)_{10}(DUPHOS)]$ (**3**), 1,1-$[H_4Ru_4(CO)_{10}(O\text{-}DUPHOS)]$ (**4**), 1,2-$[H_4Ru_4(CO)_{10}(DIOP)]\cdot 0.6CHCl_3$ (**5**), $[\{H_4Ru_4(CO)_{10}(DIOP)\}_2]\cdot 1.6C_6H_{14}$ (**6**) and 1,1-$[H_4Ru_4(CO)_{10}(DIPAMP)]\cdot 0.4H_2O$ (**7**)

Compound	**1** $C_{33}H_{33}O_{11}PRu_4$	**2** $C_{54}H_{62}O_{10}P_2Ru_4\cdot CH_2Cl_2$	**3** $C_{28}H_{32}O_{10}P_2Ru_4$	**4** $C_{28}H_{32}O_{11}P_2Ru_4$	**5** $C_{41}H_{36}O_{12}P_2Ru_4\cdot 0.6CHCl_3$	**6** $C_{82}H_{72}O_{24}P_4Ru_8\cdot 1.6C_6H_{14}$	**7** $C_{38}H_{32}O_{12}P_2Ru_4\cdot 0.4H_2O$
M	1040.84	1422.18	994.76	1010.76	1306.29	2460.01	1162.86
T/K	120(2)	120(2)	293(2)	120(2)	293(2)	293(2)	293(2)
λ/Å	0.71073	0.71073	0.71073	0.71073	0.71073	0.71073	0.71073
Crystal symmetry	Orthorhombic	Monoclinic	Orthorhombic	Monoclinic	Orthorhombic	Monoclinic	Orthorhombic
Space group	$P2_12_12_1$ (no. 19)	$P2_1$ (no. 4)	$P2_12_12_1$ (no. 19)	$P2_1$ (no. 4)	$P2_12_12_1$ (no. 19)	$P2_1$ (no. 4)	$P2_12_12_1$ (no. 19)
a/Å	9.3074(1)	9.309(2)	11.651(2)	9.727(2)	12.7512 (2)	15.9624(5)	11.8868(4)
b/Å	17.7513(3)	19.380(4)	15.180(3)	16.058(3)	18.7601 (4)	19.8385(6)	16.0305(6)
c/Å	22.3268(3)	15.867(3)	38.529(8)	12.132(2)	21.1114 (4)	17.5353(5)	22.8822(8)
β/°	90	90.51(3)	90	113.35(3)	90	106.296(1)	90
V/Å^3	3689(1)	2862(1)	6814(2)	1739.9(6)	5050.1(2)	5329.8(3)	4360.2(3)
Z	4	2	8	2	4	2	4
D_c/Mg m^{-3}	1.874	1.650	1.939	1.929	1.718	1.533	1.771
μ(Mo-Kα)/mm^{-1}	1.71	1.24	1.884	1.85	1.450	1.224	1.492
F(000)	2040	1428	3888	988	2568	2436	2280
Crystal size/mm	0.40 × 0.20 × 0.10	0.30 × 0.10 × 0.10	0.30 × 0.10 × 0.10	0.25 × 0.25 × 0.20	0.30 × 0.15 × 0.10	0.40 × 0.20 × 0.10	0.30 × 0.23 × 0.20
θ limits/°	3–27	4–27	3–26	2–26	1–30	3–28	2–30
Reflections collected, hkl	41845	12823	13756	7035	69624	61602	57874
Unique observed reflections [$F_o > 4\sigma(F_o)$]	8385	12823	13756	7035	14751	25688	13019
Goodness of fit on F^2	1.072	1.086	1.033	1.090	0.794	0.802	1.086
R_1 (F)[a]	0.0226	0.0169	0.0428	0.0181	0.0422	0.0452	0.0411
wR_2 (F^2)[b]	0.0427	0.0399	0.0615	0.0433	0.0792	0.0893	0.0976
Weighting scheme	$a = 0.0139$, $b = 0.5566$[b]	$a = 0.0000$, $b = 0.6777$[b]	$a = 0.0000$, $b = 4.2044$[b]	$a = 0.0000$, $b = 0.0961$[b]	$a = 0.0336$, $b = 0.0000$[b]	$a = 0.0600$, $b = 8.1281$[b]	$a = 0.0366$, $b = 7.5109$[b]
Largest diff. peak, hole/e Å^{-3}	0.360, −0.617	0.362, −0.421	0.697, −0.601	0.489, −0.671	0.691, −0.971	0.600, −0.828	0.952, −1.079
Absolute structure parameter	−0.03(2)	−0.02(1)	−0.01(3)	0.0024(2)	−0.05(3)	−0.01(2)	−0.02(4)

[a] $R_1 = \sum\|F_o| - |F_c|/\sum|F_o|$. [b] $wR_2 = [\sum w(F_o^2 - F_c^2)^2/\sum w(F_o^2)^2]^{1/2}$ where $w = 1/[\sigma^2(F_o^2) + (aP)^2 + bP]$ where $P = (F_o^2 + 2F_c^2)/3$.

(**7**), containing a five-membered chelate ring, and only a fraction of 1,2-[$H_4Ru_4(CO)_{10}$(DIPAMP)] (**8**), which contains a six-membered "dimetallacycle". On the other hand, oxidative decarbonylation gave mainly cluster **8** with a small quantity of **7**. The combined yields of **7** and **8** were found to be roughly the same for both these methods. It was found that **8** slowly converts into **7** in solution, probably because of the relative ring strain present in **8**. Thus, attempts to crystallize **8** invariably resulted in a mixture of **7** and **8**. A slow increase of the concentration of **7** in the crystallization mixture was observed using spot TLC (CH_2Cl_2–*n*-hexane 2 : 3). This slow conversion of **8** into **7** could be monitored for several days/weeks (depending on the storage temperature for the specific sample). Keeping the compound(s) in solution for such a relatively long period of time resulted in (competing) cluster decomposition, as evidenced by a brown stationary spot in the spot TLC that increased in intensity with time. The interconversion of **8** into **7** is very similar to that which has been established previously for the directly analogous isomers of [$H_4Ru_4(CO)_{10}$(dppe)],[17] which are essentially isostructural to **7** and **8**.

General description of the crystal structures of clusters 1–7

All clusters investigated by single-crystal X-ray diffraction are based on the tetrahedral geometry of the metal frameworks and all clusters obey the EAN rule (60 valence electrons). The coordination geometry of the Ru_4 tetrahedra are completed by four bridging hydrides, eleven or ten terminal carbonyl ligands and one or two monodentate chiral phosphine ligands to give [$H_4Ru_4(CO)_{11}$(NMDPP)] (**1**) and [$H_4Ru_4(CO)_{10}$(NMDPP)$_2$] (**2**), respectively. In the case of the diphosphine-substituted clusters, the chelating (1,1-[$H_4Ru_4(CO)_{10}$(DUPHOS)] (**3**), 1,1-[$H_4Ru_4(CO)_{10}$-(O-DUPHOS)] (**4**) and 1,1-[$H_4Ru_4(CO)_{10}$(DIPAMP)] (**7**)) and bridging ([$H_4Ru_4(CO)_{10}$(DIOP)] (**5**)) or doubly bridging ([{$H_4Ru_4(CO)_{10}$(μ-DIOP)}$_2$] (**6**)) coordination modes are present (*cf.* Fig. 2) with ten terminal carbonyl ligands. In **1–7**, the CO ligands are staggered with respect to the Ru–Ru vectors in contrast to the eclipsed conformation of the carbonyls in [$H_4Re_4(CO)_{12}$] where the hydrides are face-bridging.[18] Although not all the hydrides have been directly located from the Fourier-maps, the usual pattern of two "short" and four "long" Ru–Ru separations indicate that the latter bonds are spanned by bridging hydrides. Further evidence of the positions of the hydrides is given by the orientations of the carbonyls bound to ruthenium atoms that are also connected to bridging hydrides; these carbonyl ligands are bent away from the hydride positions. In the Ru_4(μ-H)$_4$ cores, the distribution of the hydrides along the Ru–Ru edges conforms to the idealized D_{2d} symmetry (**2**, **6**) of the precursor [$H_4Ru_4(CO)_{12}$] or to C_s symmetry (**1**, **3**, **4**, **5**, **7**) in the solid state (Fig. 3). It should be pointed out that the energy difference between D_{2d} and C_s symmetry of the Ru_4(μ-H)$_4$ core is usually very small and thus, the hydrides are usually fluxional in solution at ambient temperature (*vide infra*);[19] however, exceptions to this rule are found, notably the cluster 1,1-[$H_4Ru_4(CO)_{11}$(BDPP)] which gives high enantioselectivity in asymmetric hydrogenation of tiglic acid.[8]

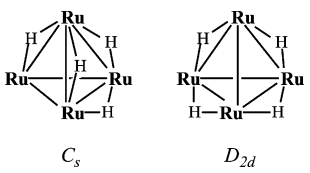

Fig. 3 Schematic depiction of the D_{2d} and C_s conformations of the Ru_4(μ-H)$_4$ cluster core.

Molecular structures of [$H_4Ru_4(CO)_{11}$(NMDPP)] (1) and [$H_4Ru_4(CO)_{10}$(NMDPP)$_2$] (2)

The molecular structures of clusters **1** and **2** are shown in Fig. 4 and 5 and relevant bond lengths and angles are reported in Table 2. In the solid state, the monosubstituted phosphine derivative **1** differs from the previously reported [$H_4Ru_4(CO)_{11}(PR_3)$] species (R = OMe,[20,21] Ph,[22,23] SC_4H_3,[24] C_6F_5,[21] OEt[21]) and dimeric [{$H_4Ru_4(CO)_{11}$}$_2$(μ-Ph_2P–C≡C–C≡C–PPh_2)][24] with respect to the symmetry of the Ru_4(μ-H)$_4$ core which becomes C_s instead of D_{2d}. This lower symmetry arrangement of the edge bridging hydrides has been found only in [$H_4Ru_4(CO)_{11}(PMe_2Ph)$][21] and in both cases the ruthenium bearing the phosphine is that bound to three bridging hydrides and transoid to one of the short Ru–Ru vectors. The *trans* Ru(1)–Ru(3)–P(1) angle deviates more

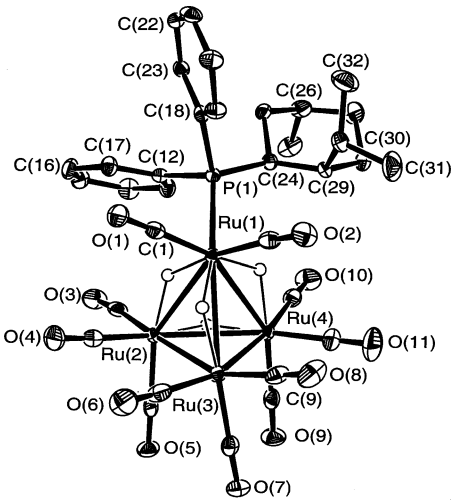

Fig. 4 An ORTEP drawing of the molecular structure of [$H_4Ru_4(CO)_{11}$(NMDPP)] (**1**) showing the atom numbering scheme. Thermal ellipsoids are drawn at the 30% probability level. For the sake of clarity, all hydrogen atoms except the hydrides have been omitted.

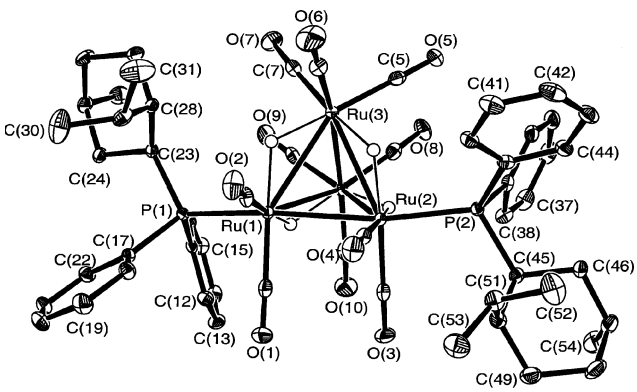

Fig. 5 An ORTEP drawing of the molecular structure of [$H_4Ru_4(CO)_{10}$(NMDPP)$_2$] (**2**) showing the atom numbering scheme. Thermal ellipsoids are drawn at the 30% probability level. For the sake of clarity, all hydrogen atoms except the hydrides have been omitted.

Table 2 Selected bond lengths (Å) and angles (°) for $[H_4Ru_4(CO)_{11}(NMDPP)]$ (**1**), $[H_4Ru_4(CO)_{10}(NMDPP)_2]\cdot CH_2Cl_2$ (**2**), 1,1-$[H_4Ru_4(CO)_{10}(DUPHOS)]$ (**3**), 1,1-$[H_4Ru_4(CO)_{10}(O\text{-}DUPHOS)]$ (**4**) and 1,2-$[H_4Ru_4(CO)_{10}(DIOP)]\cdot 0.6CHCl_3$ (**5**)

	1	**2**	**3**[a]	**4**	**5**	**7**
Ru(1)–Ru(2)	2.9693(3)[b]	2.790(1)	2.994(1)[b](A), 2.959(1)[b] (B)	2.895(1)[b]	3.0295(7)[b]	2.9796(6)[b]
Ru(1)–Ru(3)	2.9720(3)[b]	2.962(1)[b]	2.932(1)[b] (A), 3.058(1)[b] (B)	3.029(1)[b]	2.9894(7)[b]	3.0439(6)[b]
Ru(1)–Ru(4)	3.0069(3)[b]	3.005(1)[b]	3.038(1)[b] (A), 2.956(1)[b] (B)	3.015(1)[b]	3.0245(7)[b]	2.9570(6)[b]
Ru(2)–Ru(3)	2.7765(3)	2.977(1)[b]	2.801(1) (A), 2.786(1) (B)	2.783(1)	2.7823(7)	2.9396(6)[b]
Ru(2)–Ru(4)	2.9162(3)[b]	2.952(1)[b]	2.911(1)[b](A), 2.805(1)[b] (B)	2.779(1)	2.9448(7)[b]	2.7935(6)
Ru(3)–Ru(4)	2.7830(3)	2.789(1)	2.789(1) (A), 2.943(1) (B)	2.939(1)[b]	2.7803(7)	2.7823(6)
Ru(1)–P(1)	2.372(1)	2.383(1)	2.306(2) (A), 2.311(2) (B)	2.297(1)	2.357(2)	2.325(1)
Ru(1)–P(2)[c]			2.314(2) (A), 2.305(2) (B)	2.140(2)		2.303(2)
Ru(2)–P(2)		2.377(1)			2.360(2)	
P(1)–Ru(1)–P(2)[c]			83.70(6) (A), 85.28(6) (B)	85.61(6)		85.20(5)
Ru(1)–P(1)–C(31)[c]			108.0(2) (A), 109.5(2) (B)	113.2(1)		
Ru(1)–P(2)–C(36)			108.9(2) (A), 109.0(2) (B)			
Ru(1)–O(1)–P(2)				121.9(1)		

[a] Two independent molecules are present in the crystal of complex **3** (A and B). [b] Ru–Ru bonds bridged by hydrides. [c] P(2)=O(1) for **4**. [d] C(31)=C(76) for **4**.

from linearity [159.84(2)°] than the analogous angles in the three aforementioned species and is strictly comparable to the value found in $[H_4Ru_4(CO)_{11}(PMe_2Ph)]$[21] [159.03(5)°]. The disubstituted cluster $[H_4Ru_4(CO)_{10}(NMDPP)_2]$ (**2**) adopts a D_{2d} geometry of the $Ru_4(\mu\text{-}H)_4$ core with the two phosphines transoid to the same short (unbridged) Ru–Ru bond [Ru(1)–Ru(2) 2.790(1) Å] as has been found in $[H_4Ru_4(CO)_{10}(PPh_3)_2]$[25] and in $[H_4Ru_4(CO)_{10}(PFu_3)_2]$[26] (Fu = furyl). Interestingly, the latter cluster exhibits also an isomer which differs with regard to the phosphine positions that are transoid to two different short Ru–Ru interactions, as has been observed in $[H_4Ru_4(CO)_{10}(POEt_3)_2]$.[19]

Molecular structures of 1,1-$[H_4Ru_4(O)_{10}(DUPHOS)]$ (3) and $[H_4Ru_4(CO)_{10}(O\text{-}DUPHOS)]$ (4)

Cluster **3**, which is shown in Fig. 6 (relevant bond lengths and angles are reported in Table 3), has a DUPHOS ligand

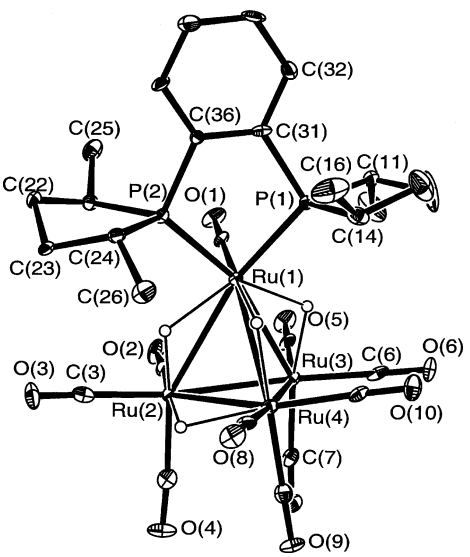

Fig. 6 An ORTEP drawing of the molecular structure of 1,1-$[H_4Ru_4(CO)_{10}(DUPHOS)]$ (**3**) showing the atom numbering scheme. Thermal ellipsoids are drawn at the 30% probability level. For the sake of clarity, all hydrogen atoms except the hydrides have been omitted.

Table 3 Selected bond lengths (Å) for $[\{H_4Ru_4(CO)_{10}(DIOP)\}_2]\cdot 1.6C_6H_{14}$ (**6**)

Ru(1)–Ru(2)	2.9839(6)	Ru(5)–Ru(8)	2.7918(6)
Ru(1)–Ru(3)	2.7941(5)	Ru(6)–Ru(7)	2.7941(5)
Ru(1)–Ru(4)	2.9808(6)	Ru(6)–Ru(8)	2.9931(6)
Ru(2)–Ru(3)	2.9719(5)	Ru(7)–Ru(8)	2.9476(6)
Ru(2)–Ru(4)	2.7857(6)	Ru(5)–Ru(7)	2.9790(6)
Ru(3)–Ru(4)	2.9616(6)	Ru(5)–Ru(6)	2.9914(6)
P(1)–Ru(1)	2.357(2)	P(2)–Ru(5)	2.361(2)

chelating the ruthenium atom that is coordinated by three bridging hydrides, and adopts the C_s symmetry of the $Ru_4(\mu\text{-}H)_4$ core that is usually found in the case of chelating and bridging diphosphines. It crystallizes with two independent molecules in the asymmetric unit that mostly differ in the conformation of the five-membered RuPCCP metallacycle. This ring is planar in one molecule (maximum deviation from planarity for molecule B is 0.02 Å) and slightly skewed in the other but presumably these differences are due to packing effects. The unusual asymmetric chelating P–Ru–O–P coordination of DUPHOS in compound **4** (Fig. 7) gives bond lengths of 2.297(1), 2.140(2) and 1.511(2) Å for Ru(1)–P(1), Ru(1)–O(1) and O(1)–P(2), respectively, while the observed Ru(1)–O(1)–P(1) bond angle was 121.9(1)° (bond lengths and angles are summarized in Table 3). As expected, the bite angle of 85.6(1)° for O(1)–Ru(1)–P(1) in the six-membered chelate ring was somewhat larger than the corresponding values in the five-membered chelate rings in cluster **3** (P(1)–Ru(1)–P(2) 83.70(6)°, 85.28(6)° for molecule A and B, respectively). A similar six-membered ring consisting of a dimetallacycle formed by DUPHOS bridging an Os–Os bond has been observed in $[Os_3(CO)_{10}(\mu\text{-}DUPHOS)]$.[27]

Molecular structures of 1,2-$[H_4Ru_4(CO)_{10}(DIOP)]$ (5) and $[\{H_4Ru_4(CO)_{10}(\mu\text{-}DIOP)\}_2]$ (6)

In cluster **5** (shown in Fig. 8) the DIOP diphosphine is bridging one Ru–Ru vector giving rise to an eight-membered ring and the $Ru_4(\mu\text{-}H)_4$ core conforms to a C_s symmetry as is found in other $[H_4Ru_4(CO)_{10}(\text{diphosphine})]$ clusters. The two Ru–P distances are almost identical [2.357 and 2.360(2) Å] and the P ··· P separation

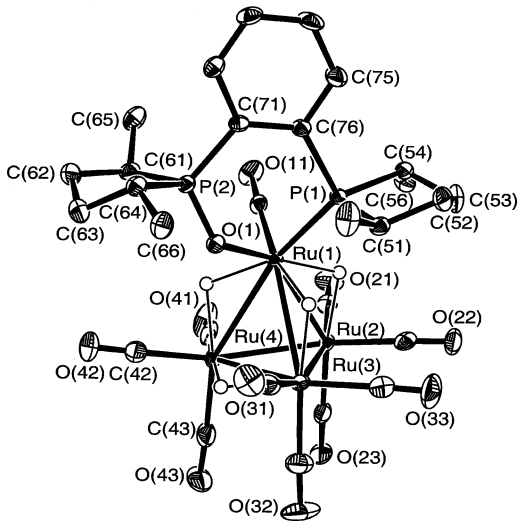

Fig. 7 An ORTEP drawing of the molecular structure of $[H_4Ru_4(CO)_{10}$-(O-DUPHOS)] (**4**) showing the atom numbering scheme. Thermal ellipsoids are drawn at the 30% probability level. For the sake of clarity, all hydrogen atoms except the hydrides have been omitted.

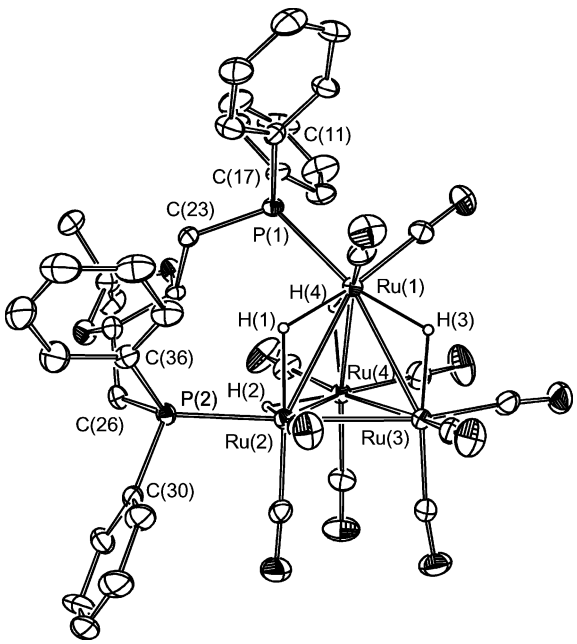

Fig. 8 An ORTEP drawing of the molecular structure of 1,2-$[H_4Ru_4$-$(CO)_{10}$(DIOP)] (**5**) showing the atom numbering scheme. Thermal ellipsoids are drawn at the 30% probability level. For the sake of clarity, all hydrogen atoms except the hydrides have been omitted.

[4.870(2) Å] compares well to the value found in another tetranuclear cluster with a bridging DIOP ligand, $[Ir_4(CO)_{10}(DIOP)]$[28] [4.75 Å], and in the trinuclear $[Os_3H_2(CO_8(DIOP)]$[29] [4.529(7) Å] but is much shorter than that in $[Ru_3(CO)_{10}(DIOP)]$ [5.09 Å]. The solid state structure of **6** (Fig. 9) consists of two tetrahedral $H_4Ru_4(CO)_{10}$ units linked together by two diphosphines bridging the two cluster units, thus forming a 16-membered ring. Each tetrahedral cluster retains the D_{2d} symmetry of the H_4Ru_4 core typical of the parent $[H_4Ru_4(CO)_{12}]$ and most of the $[H_4Ru_4(CO)_{11}(PR_3)]$ and $[H_4Ru_4(CO)_{10}(PR_3)_2]$ clusters (*vide supra*). In addition, the

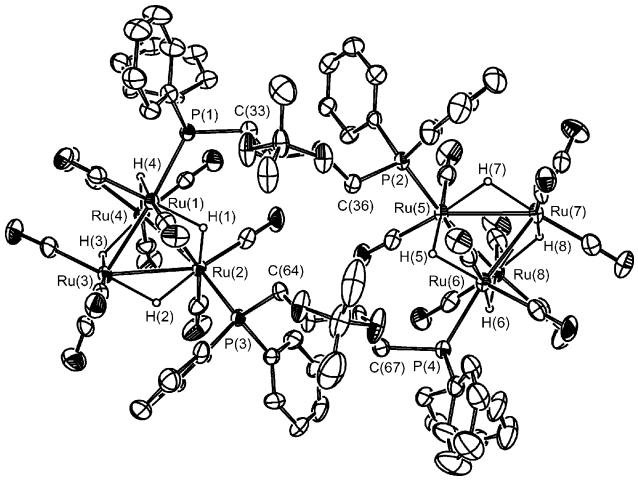

Fig. 9 An ORTEP drawing of the molecular structure of $[\{H_4Ru_4$-$(CO)_{10}(\mu\text{-DIOP})\}_2]$ (**6**) showing the atom numbering scheme. Thermal ellipsoids are drawn at the 30% probability level. For the sake of clarity, all hydrogen atoms except the hydrides have been omitted.

coordination of the P atoms of the DIOP ligand to the Ru atoms is more similar to that of the phosphorus atoms in $[H_4Ru_4(CO)_{10}(POEt_3)_2]$[26] than to the analogous interaction in the related compound **5** where the diphosphine is bridging one Ru–Ru bond. The two P atoms in each cluster unit are transoid to two different short Ru–Ru vectors, as previously observed in $[H_4Ru_4(CO)_{10}(POEt_3)_2]$,[19] in order to allow further coordination using the second P atoms of the DIOP ligands which would be prevented by a conformation similar to that in **2**. Another effect of this unusual coordination of the diphosphine resides in the long P···P separations in each DIOP unit [P(1)···P(2) 6.51 and P(3)···P(4) 6.30 Å, respectively] compared to a distance of 4.87 Å in **5** but very close to the separations found in the polymeric $[Ag(NO_3)(DIOP)]_n$[30] and dinuclear $[\{OsH_2(PiPr_3)_2\}_2(\mu\text{-DIOP})]$[31] complexes [6.79 and 6.63 Å, respectively].

Molecular structure of 1,1-$[H_4Ru_4(CO)_{10}$(DIPAMP)] (7)

In the cluster 1,1-$[H_4Ru_4(CO)_{10}$(DIPAMP)] (**7**) (shown in Fig. 10) the $Ru_4(\mu\text{-H})_4$ core conforms to C_s symmetry and the chelating coordination mode of the diphosphine generates a five-membered ring with a P(1)–Ru(1)–P(2) bite angle of 85.20(5)° which is almost identical to that found in cluster **3** (*vide infra*) containing the five-membered DUPHOS ligand. The conformation of the five-membered RuPCCP ring is δ and the absolute configuration of the two P atoms becomes *S*,*S* by coordination. The chiral DIPAMP ligand displays an edge-face edge-face chiral conformation of the phenyl and *o*-anisyl groups in addition to the chirality imposed by the P atoms. The oxygen atom of the *o*-anisyl group points towards the Ru(1) centre but no bonding interactions are present [Ru(1)···O(12) 3.77, Ru(1)···O(11) 3.96 Å].

A number of previous studies have shown that the hydrides in $[H_4Ru_4(CO)_{12}]$ and its derivatives are fluxional; variable temperature ^1H and ^{31}P NMR measurements have revealed hydride scrambling pathways both for bridging and chelating diphosphine derivatives.[3b,17,32] In clusters **1** and **2**, the observed hydride resonances are fairly sharp in contrast to the significantly broadened signals in 1,1-$[H_4Ru_4(CO)_{10}$(DUPHOS)] (**3**), which again indicates

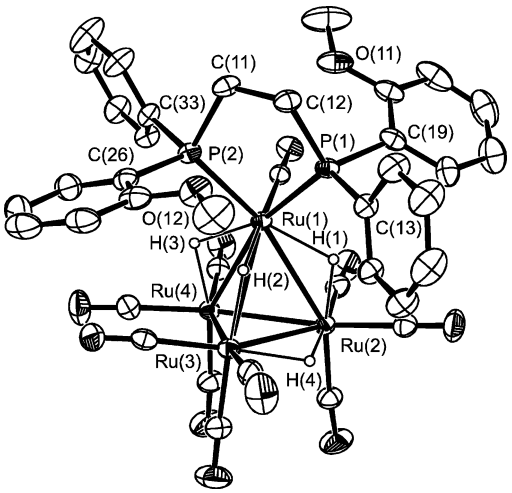

Fig. 10 An ORTEP drawing of the molecular structure of 1,1-$[H_4Ru_4(CO)_{10}(DIPAMP)]$ (**7**) showing the atom numbering scheme. Thermal ellipsoids are drawn at the 30% probability level. For the sake of clarity, all hydrogen atoms except the hydrides have been omitted.

tautomerization between the various edge-bridging hydride positions on the Ru_4 tetrahedron. In addition to these resonances, a fairly sharp triplet at −19.6 ppm is found for cluster **3**, which may be assigned as the hydride located *cis* to both phosphines, *i.e.* spanning Ru(1) and Ru(4) in Fig. 6. A variable temperature NMR study[32] on $[H_4Ru_4(CO)_{10}(dppe)]$ has shown the non-fluxional character of this hydride. In the solid state, identical hydride locations are found for cluster **3**; in both molecules A and B the basal hydrides coordinate similar Ru–Ru edges, *i.e.* Ru(2)–Ru(4) in Fig. 6. Although variable temperature investigations have not been carried out, the ^{31}P NMR measurements are fully consistent with the observed solid-state structures for **1–3**, suggesting that the phosphine ligands do not give rise to fluxionality or existence of other isomeric structures in these clusters. In the case of the DIOP-containing clusters **5** and **6**, the ^{31}P NMR spectra indicated the existence of conformers for the former and stereochemical nonrigidity (on the NMR time scale) for the latter. Furthermore, the above-mentioned isomerization of **8** to **7** could be detected *via* ^{31}P NMR spectroscopy.

Asymmetric hydrogenation of tiglic acid

Most successful asymmetric catalytic hydrogenations involving both mono- and polynuclear ruthenium compounds have been carried out with diphosphine-derivatized species;[1,33] in this study, monodentate phosphine derivatives were also tested as potential catalysts. The catalysis experiments were carried out at a relatively modest H_2 pressure of 50 bar, instead of the high H_2 pressure (130 bar) commonly used in cluster-based catalysis tests. The lower pressure was expected to enhance the chiral induction, as demonstrated in our previous study with BDPP derivatives.[8] Severe decomposition of the cluster derivatives was observed when temperatures above 120 °C were used. At these temperatures, heterogeneous black solid particles were formed and these appeared to be responsible for the catalytic action which led to the formation of considerable amounts of cyclohexenes and cyclohexane in addition to the desired 2-methyl butyric acid, as evidenced by GC-MS analyses. When lower temperatures were used, all reaction mixtures remained homogeneous, and the above-mentioned hydrogenation products of toluene were not detected. In order to obtain reasonable conversions, a temperature of 100 °C and longer reaction times of 72 h were required (conversion rates were found to decrease appreciably below *ca.* 80 °C).

The results for the catalysis tests for complexes **1–3**, **5**, **7**, **8** (cluster **4** was not tested because of the exceedingly low yield) are presented in Table 4. All clusters yielded moderate to low conversions, even when extended reaction times (72 h) and substrate to catalyst molar ratios of 250 to 500 were used. After catalysis runs, clusters **1** and **3**, and **7**/**8** could be recovered unaltered with *ca.* 50% yields. As was found in our study of hydrogenation catalyzed by $[H_4Ru_4(CO)_{10}(BDPP)]$,[8] and in our efforts to crystallize cluster **8** (*vide supra*), the didentate DIPAMP ligand in **8** changes its coordination mode from bridging two different Ru metal atoms into the more energetically favored chelating coordination mode, thus forming **7** during the catalytic tests. This was found to have no apparent influence on the results of the catalytic experiments, w.r.t. efficiency, regio- and enantioselectivity. The same results were obtained regardless of whether cluster **7** or **8** was used as the initial catalyst.

For both $[H_4Ru_4(CO)_{10}(NMDPP)_2]$ (**2**) and 1,2-$[H_4Ru_4(CO)_{10}(DIOP)]$ (**5**), partial decomposition of the catalyst was observed. In several tests, the final reaction mixtures obtained from catalysis by **2** contained both the mono- and disubstituted species **1** and **2**, respectively. Nevertheless, the observed conversion rates remained low in most experiments, the decomposition causing only slightly larger deviations to the product distributions, *i.e.* formation of 2-methyl-2-butenoate. Larger deviations of the product distribution could be observed for clusters **7**/**8**, even though very little cluster decomposition was detected.

Table 4 Asymmetric catalytic hydrogenation of tiglic acid in the presence of tetranuclear ruthenium hydrido clusters

Catalyst/mg	R^a/react. time (h)	Conversion (%)	Selectivity[b] (%)	ee (%)	Configuration
$[H_4Ru_4(CO)_{12}]$/5	250/48	21	99	—	—
1/5	250/48	13	98	—	—
1/5	250/72	32	97	11	*R*
2/5	250/48	29	100	—	—
2/5	250/72	42–68	97–99	6	*R*
3/5	300/48	23	100	—	—
3/5	300/72	13–24	97–99	5–11	*R*
5/10	500/24	70–95	92–93	10–23	*S*
7, **8**[c]/10	500/24	49–98	89	0	—

[a] $R = n$(substrate)/n(catalyst), $p(H_2) = 50$ bar, $T = 100$ °C, solvent = EtOH–toluene 1 : 1 [5 mL ($R = 250$); 6 mL ($R = 500$)]. [b] 2-Methyl-2-butenoate is also formed. [c] Isomerization between **7** and **8** is observed (see text).

While reasonable improvements in conversion rates relative to the parent cluster $[H_4Ru_4(CO)_{12}]$ could be observed for clusters **1**, **2**, **5** and **7**/**8**, relatively low enantiomeric excesses were observed (5–23%) and in the case of **7**/**8** no enantioselectivity could be detected. These results indicate weak interactions between the substrate and these cluster derivatives. Furthermore, the catalytic inefficiency of the possible decomposition products under the used reaction conditions provides indirect evidence that the cluster species may be the actual catalysts.[8] Both the catalytic activity and the chiral induction appear to be mainly dependent on the chemical nature of the phosphine ligand used, although the exact reaction mechanism for the cluster-based catalytic hydrogenation is still uncertain.[8]

In order to obtain reasonable chiral induction, it is likely that bulkier phosphine ligands must be used to introduce the chirality to cluster derivatives of $[H_4Ru_4(CO)_{12}]$. This has been demonstrated by the results obtained with cluster derivatives of BINAP[7a] and BDPP,[8] where the chiral centers are in the vicinity of phosphine-coordinated phenyl rings. It is likely that these groups also suitably modify the electronic properties of the cluster core to establish efficient catalytic cycles.

Conclusions

In summary, we have synthesized and characterized eight new chiral tetranuclear ruthenium clusters containing the ligands NMDPP, DUPHOS, DIOP and DIPAMP, and we have tested their behaviour in asymmetric catalytic hydrogenation of tiglic acid. On the basis of these results and those obtained in previous investigations, it appears that the cluster-coordinated phosphines play a key role for the performance of these catalysts. The best results are obtained when the parent cluster $[H_4Ru_4(CO)_{12}]$ is derivatized with sterically demanding didentate phosphines such as BDPP or BINAP, which additionally favour the chelating coordination mode. We are currently trying to use *in situ* high-pressure spectroscopic methods to investigate catalytic hydrogenation reactions that involve these types of clusters.

Acknowledgements

This research has been sponsored by the Swedish Research Council (VR), the European Union TMR network Metal Clusters in Catalysis and Organic Synthesis, the Nordic Council of Ministers, University of Bologna (M. M., S. S.) and MIUR (M. M. and S. S.). We thank Prof. Carlaxel Andersson for the generous loan of an autoclave.

References

1 W. S. Knowles, *Angew. Chem., Int. Ed.*, 2002, **41**, 1998; W. S. Knowles, *Acc. Chem. Res.*, 1983, **16**, 106.
2 (*a*) M. J. Burk, M. F. Gross and J. P. Martinez, *J. Am. Chem. Soc.*, 1995, **117**, 9375–9376; (*b*) M. J. Burk, Y. M. Wang and J. R. Lee, *J. Am. Chem. Soc.*, 1996, **118**, 5142–5143.
3 (*a*) T. Ohta, H. Takaya, M. Kitamura, K. Nagai and R. Noyori, *J. Org. Chem.*, 1987, **52**, 3176; (*b*) T. Ohta, H. Takaya and R. Noyori, *Inorg. Chem.*, 1988, **27**, 566; (*c*) H. Takaya, T. Ohta, K. Mashima and R. Noyori, *Pure Appl. Chem.*, **62**, 1135.
4 (*a*) D. Braga, U. Matteoli, P. Sabatino and A. Scrivanti, *J. Chem. Soc., Dalton Trans.*, 1995, 419; (*b*) J. Puga, A. Arce, D. Braga, N. Centritto, F. Grepioni, R. Castillo and J. Ascanio, *Inorg. Chem.*, 1987, **26**, 867; (*c*) U. Matteoli, P. Frediani, M. Bianchi, C. Botteghi and S. Gladiali, *J. Mol. Catal.*, 1981, **12**, 281; (*d*) U. Matteoli, G. Menchi, P. Frediani, M. Bianchi and F. Piacenti, *J. Organomet. Chem.*, 1985, **285**, 281.
5 U. Matteoli, M. Bianchi, P. Frediani, G. Menchi, C. Botteghi and M. Marchetti, *J. Organomet. Chem.*, 1984, **263**, 243.
6 F. Piacenti, P. Frediani, U. Matteoli, G. Menchi and M. Bianchi, *Chim. Ind. (Milan)*, 1986, **68**, 53.
7 (*a*) U. Matteoli, V. Beghetto and A. Scrivanti, *J. Mol. Catal. A.*, 1996, **109**, 45; (*b*) A. Salvini, P. Frediani, M. Bianchi, F. Piacenti, L. Pistolesi and L. Rosi, *J. Organomet. Chem.*, 1999, **582**, 218.
8 P. Homanen, R. Persson, M. Haukka, T. A. Pakkanen and E. Nordlander, *Organometallics*, 2000, **19**, 5568.
9 S. A. R. Knox, W. J. Koepke, M. A. Andrews and H. D. Kaez, *J. Am. Chem. Soc.*, 1975, **97**, 3942.
10 E. Tyrrell, M. W. H. Tsang, G. A. Skinner and J. Fawcett, *Tetrahedron*, 1996, **52**, 9841.
11 Z. Otwinowski and W. Minor, *Methods Enzymol.*, 1997, **276**, 307–326.
12 A. Altomare, C. Cascarano, C. Giacovazzo, A. Guagliardi, A. G. G. Moliterni, M. C. Burla, G. Polidori, M. Camalli and R. Spagna, *SIR97, A Package for Crystal Structure Solution by Direct Methods and Refinement*, University of Bari, Italy, 1997.
13 G. M. Sheldrick, *SHELXS97, Program for Crystal Structure Determination*, University of Göttingen, Germany, 1997.
14 G. M. Sheldrick, *SHELXL97, Program for Crystal Structure Refinement*, University of Göttingen, Germany, 1997.
15 A. G. Orpen, XHYDEX, *J. Chem. Soc., Dalton Trans.*, 1980, 2509.
16 H. D. Flack, *Acta Crystallogr., Sect. A.*, 1983, **39**, 876.
17 M. R. Churchill, R. A. Lashewycz, S. I. Richter and J. R. Shapley, *Inorg. Chem.*, 1980, **19**, 1277.
18 R. D. Wilson, S. M. Wu, R. A. Love and R. Bau, *Inorg. Chem.*, 1978, **17**, 1271, and references therein.
19 S. Aime, M. Botta, R. Gobetto, L. Milone, D. Osella, R. Gellert and E. Rosenberg, *Organometallics*, 1995, **14**, 3693.
20 R. D. Wilson and R. Bau, *J. Am. Chem. Soc.*, 1976, **98**, 2434.
21 M. G. Ballinas-López, E. V. García-Báez and M. G. Rosales-Hoz, *Polyhedron*, 2003, **22**, 3403.
22 R. D. Wilson and R. Bau, *J. Am. Chem. Soc.*, 1976, **98**, 4687.
23 A. U. Härkönen, M. Ahlgrén, T. A. Pakkanen and J. Pursiainen, *J. Organomet. Chem.*, 1997, **530**, 191.
24 T. M. Räsänen, S. Jääskelainen and T. A. Pakkanen, *J. Organomet. Chem.*, 1998, **553**, 453.
25 C. J. Adams, M. I. Bruce, E. Horn, B. W. Skelton, E. R. T. Tiekink and A. H. White, *J. Chem. Soc., Dalton Trans.*, 1993, 3299.
26 W.-Y. Wong, F.-L. Ting and Z. Lin, *Organometallics*, 2003, **22**, 5100.
27 S. Selva, PhD Thesis, University of Bologna, 2001.
28 D. Tranqui, A. Durif, M. N. Eddine, J. Lieto, J. J. Rafalko and B. C. Gates, *Acta. Crystallogr., Sect. B*, 1982, **38**, 1916.
29 M. J. Stchedroff, V. Moberg, E. Rodriguez, A. E. Aliev, J. Böttcher, J. W. Steed, E. Nordlander, M. Monari and A. J. Deeming, *Inorg. Chim. Acta*, DOI: 10.1016/j.ica.2005.06.048, in press.
30 B. Wu, W.-J. Zhang and S.-Y. Yu, *J. Chem. Soc., Dalton Trans.*, 1997, 1795.
31 C. Schlünker, M. E. Esteruelas, F. J. Lahoz, L. A. Oro and H. Werner, *Eur. J. Inorg. Chem.*, 2004, 2477.
32 J. R. Shapley, S. I. Richter, M. R. Churchill and R. A. Lashewycz, *J. Am. Chem. Soc.*, 1977, **99**, 7384.
33 R. D. Adams and F. A. Cotton, in *Catalysis by Di-and Polynuclear Metal Cluster Complexes*, Wiley-VCH, Weinheim, 1998.

